Dyes and Pigments 88 (2011) 25–38

Contents lists available at ScienceDirect

Dyes and Pigments

journal homepage: www.elsevier.com/locate/dyepig

An investigation of the kinetics and thermodynamics of the adsorption of a cationic cobalt porphyrazine onto sepiolite

Altuğ Mert Sevim [a], Rustam Hojiyev [b], Ahmet Gül [a,*], Mehmet Sabri Çelik [b]

[a] Department of Chemistry, Istanbul Technical University, 34469 Maslak, Istanbul, Turkey
[b] Faculty of Mines, Department of Mineral and Coal Processing, Istanbul Technical University, 34469 Maslak, Istanbul, Turkey

ARTICLE INFO

Article history:
Received 4 March 2010
Received in revised form
21 April 2010
Accepted 26 April 2010
Available online 20 May 2010

Keywords:
Adsorption
Porphyrazine
Cationic dye
Sepiolite
Thermodynamics
Kinetics

ABSTRACT

The adsorption of [octakis(2-trimethylammoniumethylsulfanyl)-porphyrazinatocobalt]octaiodide from aqueous solution onto negatively charged sepiolite is investigated. The effects of temperature, dye and solid concentration and contact time on adsorption were evaluated. Adsorption experiments were analyzed in the light of zeta potential measurements and desorption behavior of the dye–sepiolite composite. Experimental data were analyzed using four adsorption kinetic models, of which a pseudo-second-order kinetic model was found to be superior. Experimental equilibrium data were fitted to five adsorption isotherm models, from which the free energy, enthalpy and entropy of the adsorption processes were determined. Adsorption onto sepiolite was exothermic and spontaneous. AAS and FTIR were used to elucidate the adsorption mechanism. The novel composite is considered to be useful in optical and catalytic applications.

1. Introduction

Mesoporous molecular sieve-based composites are popular materials in terms of catalysis and optical applications; therefore, their design, synthesis, characterization, property, and evaluation of these materials have gained huge attention. Mesoporous materials are not only metal ion and metal oxide clusters, embedded in the regular pore systems of the host materials, they are also considered highly as hosts in the adsorption of organic dyes and metal-organic compounds [1].

Porphyrins, porphyrazines and related macrocycles are organic compounds, which provide an extremely versatile base for a variety of applications [2,3]. Close similarity among the structures of tetrapyrrole derivatives can be summarized as follows: Naturally occurring porphyrins are cyclotetrapyrroles with –CH= bridges; porphyrazines are tetrapyrroles with tetraaza bridging groups; phthalocyanines contain additional fused benzo units to pyrroles in porphyrazines [1].The tremendous potential is derived from their photophysical and electrochemical properties, remarkable stability, and well-known structure. The applications include nonlinear optics, sensors, photosensitizers, phototherapeutics, catalysts, etc [4,5]. The interest in intercalation compounds onto clay minerals can be attributed mainly to the fact that host-guest interactions influence chemical, catalytic, electronic and optical properties of guest components [5]. These composite systems also allow easy separation from the reaction products and their re-use. Such processes are increasingly encountered under the viewpoint of environmentally friendly or "green" chemistry taking three points of unlimited natural resources into account; a) oxygen (from air) as oxidant, b) often water as solvent, c) for photooxidations, use of visible light(solar radiation) [6]. Adsorption of both phthalocyanines and porphyrins onto clays are frequently investigated in terms of their catalytic and optical applications. Examples include biomimetic oxidation of hydrocarbons by clay-intercalated metalloporphyrins and/or metallophthalocyanines [7–10], using molecular oxygen for catalytic oxidations of hydrocarbons with clay-intercalated porphyrins [11,12], photochemical hole burning of cationic porphyrins intercalated in saponite [13], removal and photodecomposition of n-nonylphenol using clay incorporated with copper phthalocyanine [14]. There have been reports of unique hybrid materials, where 5,10,15,20-tetrakis(N-methylpyridinium-4-yl)porphyrin or 5,10,15,20-tetrakis (N,N,N-trimethylanilinium-4-yl) porphyrin (TMAP) cations adsorb on the clay surface of high charge densities without aggregation and completely neutralize negative charges of the surface [15,16]. However, studies on porphyrazine/clay composites and their properties are limited.

Sepiolite is a natural clay mineral with a formula of magnesium hydrosilicate $(Si_{12})(Mg_8)O_{30}(OH)_6(OH_2)_4 \cdot 8H_2O$ [17]. Similar to

* Corresponding author. Tel.: +90 212 285 68 27; fax: +90 212 285 63 86.
E-mail address: ahmetg@itu.edu.tr (A. Gül).

0143-7208/$ – see front matter © 2010 Elsevier Ltd. All rights reserved.
doi:10.1016/j.dyepig.2010.04.011

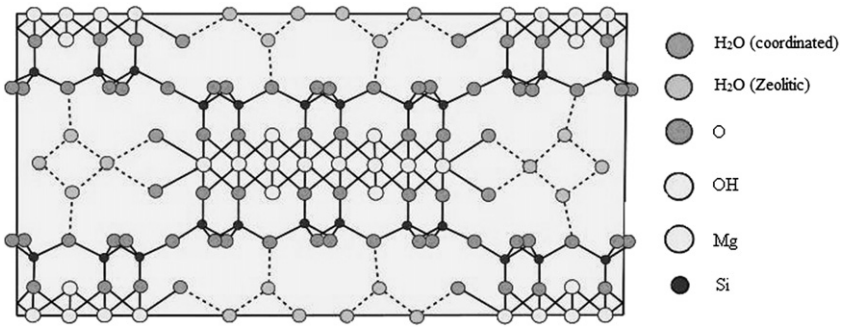

Fig. 1. Atomic lattice of sepiolite minerals.

other types of silicate minerals, it contains a continuous two-dimensional tetrahedral sheet of T_2O_5 (T = Si, Al, Be…) but has no continuous octahedral sheets (Fig. 1) [18]. This unique fibrous structure with interior channels (3.6 × 10.6 Å) allows penetration of organic and inorganic molecules and ions into the structure of sepiolite; such makes sepiolite an important industrial material in sorptive, rheological and catalytic applications [19].

This paper concersn the synthesis of a water-soluble quaternary cobalt porphyrazine and an investigation of the adsorption of this octacationic molecule (QCoPz) from aqueous solution onto negatively charged sepiolite. Equilibrium adsorption isotherms were constructed for the single component system and then the experimental data were fitted to five best known models. Experimental data were also analyzed using four adsorption kinetic models. A detailed error analysis was undertaken to investigate the effect of using different error criteria in order to obtain the best-fit isotherm and isothermal parameters which describe the adsorption process. Three different error functions were used: residual root mean square error (RMSE), average residuals (e_{ave}) and mean relative deviation modulus (E) [20]. The temperature dependence of QCoPz adsorption on sepiolite has been also investigated to calculate the thermodynamic parameters as the changes in Gibbs free energy, enthalpy and entropy of adsorption. Ion release analysis by AAS (atomic absorption spectroscopy) and FTIR techniques were used to identify the mechanism of dye adsorption. Desorption properties of the dye from the composite were also studied to further elucidate the nature of adsorption.

2. Experimental

2.1. Materials

A sepiolite sample used as an adsorbent with 85 ± 3% purity was obtained from Anatolian Industrial Minerals Company in Sivrihisar, Turkey. Chemical and mineralogical analyses of the sepiolite are presented in Tables 1 and 2, respectively. Both tables show that calcite and dolomite are the major impurities in the sample, as reported by ACME Analytical Laboratory (Inductively Coupled Plasma Spectrometer) and Dumlupınar University Geology Department Laboratory (SHIMADZU XRD-6000), respectively [21,22]. It is known that the adsorption capacity for reactive dyes increases with a decrease in particle size [23]. The sample was therefore ground to less than 150 μm which produced an average particle size (d_{50}) of 2 μm for adsorption experiments. The surface area of the sample was found to be 323 $m^2 g^{-1}$ by means of Brauner–Emmet–Teller (BET) method using (Quanto Chrome Monosorb device) helium and nitrogen as the adsorbates. The cation exchange capacity (CEC) of the sample was also found to be 0.245 meq g^{-1} by using methylene blue method. The determination of the average pore size of used sepiolite was found to be about 37 Å using Micromeritics Autopore 9220 device with mercury porosimetry [24].

Table 1
Chemical analysis of sepiolite sample used in this study.

Component	SiO_2	Al_2O_3	Fe_2O_3	MgO	CaO	Na_2O	K_2O	TiO_2	LOI
%by weight	49.85	2.38	0.87	20.15	2.65	0.10	0.36	0.13	23.50

The detailed procedures for synthesizing [octakis(2-dimethylaminoethylsulfanyl) porphyrazinatocobalt] (CoPz) have been described previously [25,26]. Cobalt porphyrazine was converted into the corresponding quaternized product (QCoPz) by reaction with iodomethane in dichloromethane. CoPz (120 mg, 0.1 mmol) was dissolved in dichloromethane (10 mL) and 1.6 mL of iodomethane was added. The ensuing mixture was stirred in the dark under a nitrogen atmosphere at room temperature for 2 days after which time, the dark blue coloured product was precipitated by centrifugation and filtered, washed with dichloromethane (2–3 times) and diethyl ether and finally dried under vacuum for 12 h. The product is water-soluble. (Yield 0.105 g; 45%). Molecular formula and molar mass of the compound are $C_{56}H_{104}N_{16}S_8I_8Co$ and 2332 g mol^{-1}. IR vibrations (cm^{-1}): 2960, 2930, 1620, 1480, 1330, 1215, 1150, 1010, 980, 910, 800, 750. UV–vis spectrum shows absorbance bands in water (λ_{max}) at 356 and 638 nm. Chemical structure of the adsorbate is given in Fig. 2. Distilled and deionized water with a conductivity value of 2×10^{-6} mho cm^{-1} was used in all experiments. Experiments were conducted at 25 °C unless otherwise specified.

2.2. Methods

The electrokinetic properties of sepiolite were determined by a Zeta Meter 3.0+ equipped with a microprocessor unit. The samples were conditioned under the adsorptive testing conditions. A sample of 50 mg of sepiolite in 50 mL of solution was shaken for 2 h followed by centrifugation for 15 min. The suspension was kept still for 5 min to let larger particles settle. About 25 mL of clear supernatant was removed from the adsorption test vial and introduced into the electrophoretic cell. An appropriate amount of sepiolite particles was pipetted out of the sepiolite bed and placed in the cell. Each data point is an average of approximately 10 measurements.

Table 2
Mineralogical analysis of sepiolite sample used in this study.

Mineral name	Formula
Sepiolite	$Mg_4Si_6O_{15}(OH)_2 \times 6H_2O$
Dolomite	$CaMg(CO_3)_2$
Albite	(Na, Ca) Al (Si, Al)$_3O_8$
Minrecordite	$CaZn(CO_3)_2$
Quartz	SiO_2
Calcite	$CaCO_3$
Montmorillonite	$Na_{0.3}(Al, Mg)_2Si_4O_{10}(OH)_2 \cdot 4H_2O$

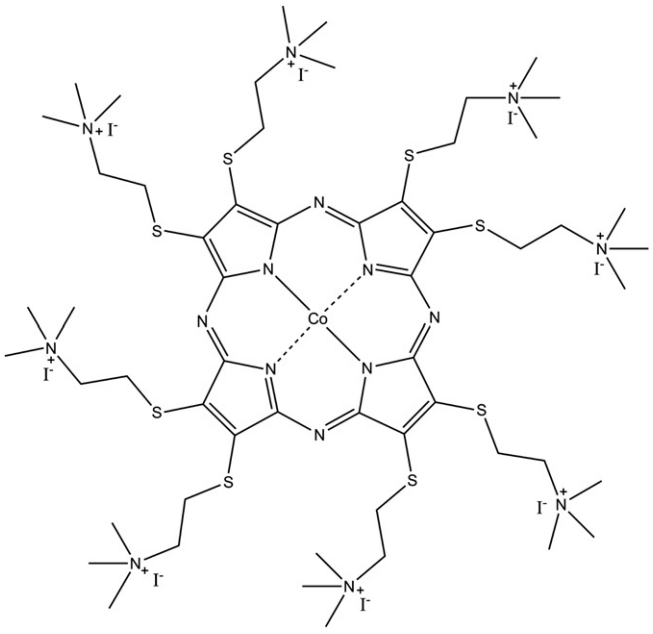

Fig. 2. Structure of [octakis(2-trimethylammoniumethylsulfanyl) porphyrazinatocobalt] octaiodide(QCoPz).

Adsorption tests were conducted in 10, 20 or 40 mL glass vials. A sepiolite sample of 10 mg was mixed in 10 mL or its multiples with solids concentration of 0.1%. The vials were shaken for 2 h in an Edmun Buhler KL2 shaker and centrifuged for 15 min. UV–vis spectrum of QCoPz shows absorbance bands in water (λ_{max}) at 356 and 638 nm. So the equilibrium concentrations of the dye were determined at 638 nm using a WTW PhotoLab visible spectrophotometer. The adsorption density was calculated by the formula given below:

$$\Gamma = (C_i - C_r)V/m1000 \quad (1)$$

In this formula, C_i and C_r represent the initial and residual concentrations in mol L^{-1}, m corresponds to the amount of solid in grams, and V is the volume of the solution in mL and finally, Γ is the adsorption density in mol g^{-1} [24].

The organo-sepiolite, formed by the adsorption of QcoPz onto sepiolite, was used in desorption studies to see whether the dye molecules are desorbed into aqueous media. The following procedure describes the experimental treatment:

20 mg of sepiolite was placed in a 20 mL flask, and 20 mL of 4 mmol L^{-1} QCoPz solution was added, and then shaken at 420 rpm for 2 h. The resulting slurries were centrifuged at 3500 rpm for 15 min, and 4 mL (20%) of aliquot was taken for analyses. The supernatant was replenished with the same amount of distilled water, and shaken again. After centrifuging for 15 min, 4 mL of aliquot was taken again, and the amount of QCoPz in the solution was calculated. This in turn was used to obtain the amount of QCoPz adsorbed by the clay. Distilled water of 4 mL was added to the flask and the above procedure was repeated until the measurement of residual concentration was no longer possible.

The infrared spectra of natural and QCoPz-adsorbed sepiolites were analyzed using Fourier transform infrared (FTIR) spectrum (Perkin Elmer Spectrum One FTIR spectrometer) to identify the functional groups responsible for the adsorption. The change of Mg^{+2} ion concentrations in solutions before and after adsorption was determined by Varian AA280 FS atomic absorption spectrophotometer.

3. Results and discussion

3.1. Effect of solids concentration

In order to determine the amount of solid to be used in adsorption experiments, a series of tests were carried out with different % solid at 1 mmol L^{-1} initial dye concentration. Examination of Fig. 3 reveals that adsorption density decreases with increasing % solid concentration and then remains practically stable. At 0.1% solid concentration, the adsorption density is 0.9247 mmol g^{-1} while the adsorption density is down to 0.0477 mmol g^{-1} at 2% solid concentration. Consequently, an optimum solid concentration of 0.1 was selected for further testing.

3.2. Change of pH during adsorption

It was observed that different concentrations of the dye yielded a constant value of pH 7.60 after the adsorption process. The natural pH of sepiolite suspension reached a pH value of 8.57 and that of QCoPz around 8 in distilled water.

3.3. Effect of mixing time

The adsorption of QCoPz onto sepiolite is presented in Fig. 4 as a function of contact time. More than 99% of QCoPz was adsorbed in

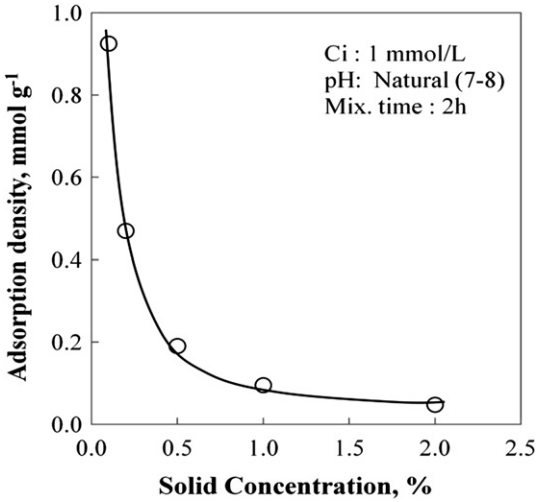

Fig. 3. Adsorption density of QCoPz vs solid concentration in sepiolite/QCoPz system.

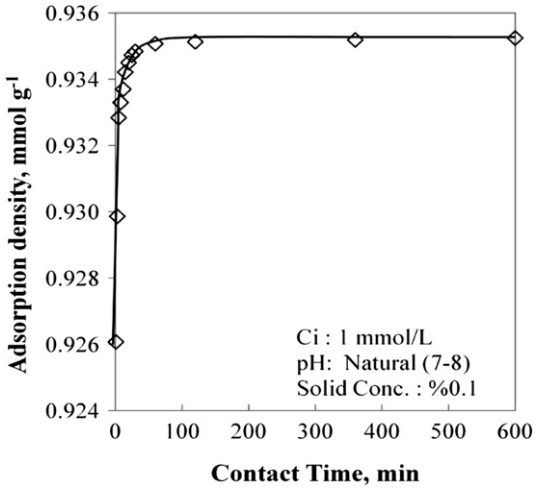

Fig. 4. Adsorption density of QCoPz versus contact time in sepiolite/QCoPz system.

about 5 min followed by a constant adsorption upon further increasing the contact time. Although the equilibrium is achieved in a short time, taking into account the effect of extreme conditions such as changes in pH, concentration, a contact time of 2 h was selected for further testing.

3.4. Electrokinetic experiments

Due to the isomorphous exchange among atoms within the clay layers, a deficiency in positive charge or, in other words, abundance in negative charge occurs. This abundance is compensated with the adsorption of cations like Na^+ and Ca^{2+} in the inter layer. In sepiolite, the negative layer charge is ascribed to the exchange of Al^{3+} and Fe^{3+} for Si^{4+} ions in the tetrahedral layers [27].

It is known from literature that there is a direct relationship between adsorption of any adsorbate onto solid surface and its corresponding zeta potential [28,29]. This fact let us to conduct a series of measurements given in Fig. 5 to determine the relationship between adsorption densities and zeta potential. As seen in the figure, pure sepiolite has a zeta potential of −14.3 mV, which means that sepiolite used in this study has a negative surface charge at natural pH of the suspension. Due to the adsorption of QCoPz onto sepiolite, an increase of zeta potential approaching a final zeta potential of +36.55 mV was observed. This change proves that cationic adsorbate adsorbed onto the negatively charged clay surface [30].

3.5. Kinetic modeling

The adsorption of organic compounds by natural materials in aqueous solution is a phenomenon with often complex kinetics due to their heterogeneous reactive surface. Since the rate of adsorption controls the residence time of adsorbate at the solid/liquid interfaces, it is an important factor for the performance of adsorption process [31].

The prediction of batch adsorption kinetics provides the most important information for designing adsorption systems [32]. Adsorption kinetics includes the search for a best model that well represents the experimental data as a function of environmental conditions.

In the present study, in order to determine the adsorption efficiency of sepiolite/QCoPz system (initial concentration = 1 mmol L^{-1}) a series of batch adsorption experiments were performed as a function of time at natural pH (7–8) and 25 °C. Then, pseudo first- and second-order, simple Elovich and intra-particle diffusion kinetic models were used to fit the experimental data.

The pseudo first-order Lagergren equation [33] is generally expressed as follows:

$$dq_t/dt = k_1(q_e - q_t) \quad (2)$$

where q_e and q_t (mmol g^{-1}) are the amounts of adsorbed dye on the adsorbent at equilibrium and at time t and k_1 is the rate constant of pseudo first-order kinetic model. After integration and applying boundary conditions $t = 0$–t and $q_t = 0$–q_t, the integrated form of equation becomes:

$$\log(q_e - q_t) = \log q_e - (k_1/2.303)t \quad (3)$$

The plots of $\log(q_e - q_t)$ against t shown in Fig. 6A for the pseudo-first-order equation give a linear relationship which k_1 and q_e values can be determined from the slope and intercept of this equation, respectively. The values of the first order model correlation coefficients together with the kinetic constants of the other used models are summarized in Table 3.

The theoretical value q_e from the first-order kinetic model gave a significantly different value compared to the experimental one, with a slightly lower correlation coefficient. Therefore, the first-order kinetic model is improper for this system.

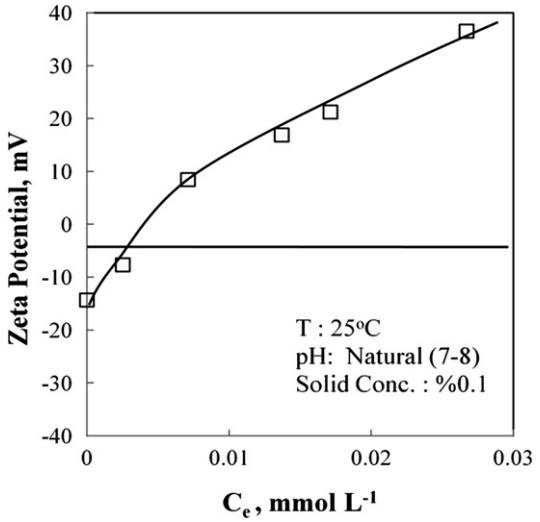

Fig. 5. The change in zeta potential with QCoPz concentration.

The kinetic data were further analyzed using pseudo second-order kinetics [34] represented as:

$$dq_t/d_t = k_2(q_e - q_t)^2 \quad (4)$$

where k_2 is the pseudo second-order rate constant (mmol g^{-1} min^{-1}), q_e and q_t are the adsorption capacity at equilibrium and at time t, respectively (mmol g^{-1}). For the boundary conditions $t = 0$ to t and $q_t = 0$–q_t, the integrated form of equation becomes:

$$t/q_t = 1/k_2qe^2 + t/q_e \quad (5)$$

where k_2qe^2 represents the initial adsorption rate. If the second-order kinetics is applicable, then the plot of t/q_t vs t should exhibit a linear relationship. The parameters (k_2 and q_e) obtained from pseudo second-order kinetic model, correlation coefficient, R^2 and experimental q_{exp} are presented in Table 3. The values of pseudo second order model parameters, q_e and k_2, were determined from the slope and intercept of t/q_t vs t plot in Fig. 6B. The calculated initial adsorption rate (k_2qe^2) of sepiolite was 0.018 mmol g^{-1} min. As can be seen from Table 3, pseudo second-order model adequately fits the data over the entire course of the experiment with the high correlation coefficient of above 98. Moreover, the experimental adsorption capacities of adsorbent are close to the theoretical values estimated from the model. Hence, the error analyses values are remarkably lower than those obtained by the application of pseudo first-order model. These findings for sepiolite/QCoPz system reveal that the adsorption process follows the pseudo second-order model.

Elovich model, which is a general application of chemisorption kinetics, assumes that the active sites of adsorbents are heterogeneous and exhibit different activation energies for the adsorption of organic compounds. Elovich model is expressed by the following equation [35];

$$dq_t/d_t = a\exp(-\beta q_t) \quad (6)$$

Among the boundary conditions $t = 0$–t and $q_t = 0$, the integrated form of equation becomes,

$$q_t = 1/\beta(\ln(\alpha\beta) + \ln t) \quad (7)$$

Eq. (7) is simplified as follows:

$$q_t = a + b\ln t \quad (8)$$

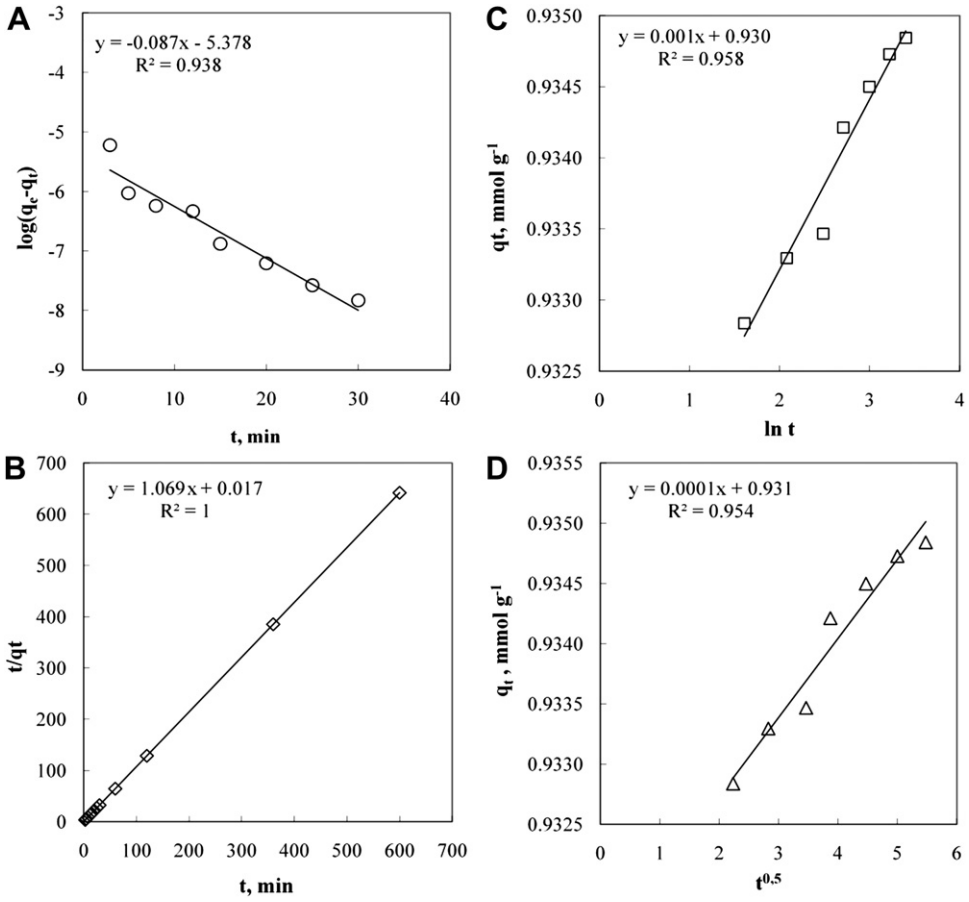

Fig. 6. Pseudo-first order (A), Pseudo-second order (B), Simple Elovich (C) and Intraparticle diffusion (D) plots of QCoPz adsorption.

The slope and intercept of the q_t vs. ln t plot shown in Fig. 6C were used to calculate the values of a and b constants in the Elovich model (Table 3); in this model, b (mmol g^{-1} min^{-1}) is the initial adsorption rate constant and a (mmol g^{-1}) is related to the extent of surface coverage and activated energy for chemisorption. The value of determination correlation coefficient for the plot was 0.77. Moreover, the calculated adsorption capacity values obtained from this kinetic model does not fit the experimental adsorption capacity values and the error analyses values are higher than those obtained from pseudo second-order model.

Lastly adsorption kinetic data were analyzed to determine whether intraparticle diffusion is rate limiting step in the adsorption process. The intraparticle diffusion approach can be described by the following equation [36]:

$$q_t = k_p\sqrt{t} \quad (9)$$

where q_t (mmol g^{-1}) is the concentration of QCoPz adsorbed at time t and k_p (mmol g^{-1} $min^{-0.5}$) is the intraparticle rate constant. This model also suggests that the adsorption process is considered to be controlled by the internal diffusion with a minor effect of the external diffusion [37]. The fraction of QCoPz uptake against square root of contact time ($t^{0.5}$) is shown in Fig. 6D. This figure reveals that the straight line obtained for sepiolite does not pass through the origin. It was suggested that this occurs when external diffusion is dominant and intraparticle diffusion is not a rate limiting step [38]. In this case, the following equation is used to describe the model:

$$q_t = k_p\sqrt{t} + C \quad (10)$$

where C is the intercept and also gives an idea about the thickness of boundary layer (Table 3), i.e. the larger the intercept the greater is the boundary layer effect [39].

Fig. 7 compares the experimental and predicted q_e values for sepiolite. As can be seen from the data, pseudo second-order model provides the best fit to sepiolite/QCoPz system for the whole contact time period with the highest correlation constant and lowest error values.

Table 3
Experimental and predicted adsorption kinetics of QCoPz by sepiolite.

Model	Constants	Clay	Model	Constants	Clay
		Sepiolite			Sepiolite
Pseudo first-order	q_e (mmol g^{-1})	4.62E−03	Simple Elovich	A	9.31E−01
	K_1 min^{-1}	8.73E−02		B	1.20E−03
	R^2	9.41E−01		R^2	7.77E−01
	E	9.29E−01		E	2.71E−03
	e ave	9.29E−01		e ave	−8.46E−04
	RMSE	8.64E−01		RMSE	2.11E−06
Pseudo second-order	q_e(mmol g^{-1})	9.36E−01	Intraparticle diffusion	K_p	7.00E−04
	K_2	2.01E−02		C	9.31E−01
	R^2	9.85E−01		R^2	9.42E−01
	E	1.55E−04		E	2.71E−03
	e ave	−1.89E−05		e ave	−2.69E−03
	RMSE	7.00E−08		RMSE	2.45E−05

3.6. Equilibrium modeling

The shape of an isotherm may predict if an adsorption system is “favorable” or “unfavorable”. The isotherm shape can also provide

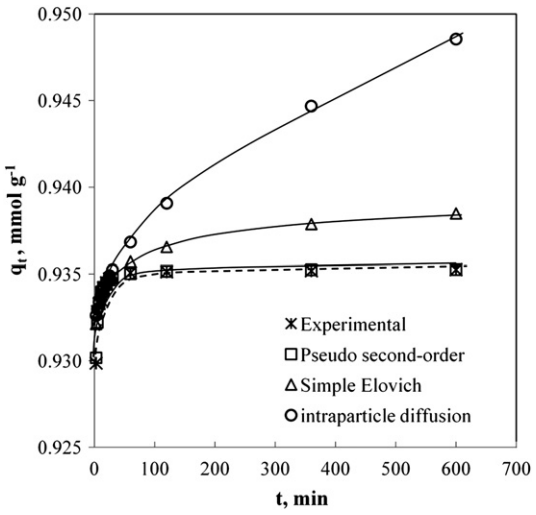

Fig. 7. Comparison of experimental and estimated adsorption kinetics of QCoPz.

qualitative information on the nature of the solute–surface interactions. In addition, adsorption isotherms are developed to evaluate the capacity of a material for the adsorption of a particular adsorbate or dye molecule [40].

The adsorption isotherms of sepiolite/QCoPz system at different temperatures are shown in Fig. 8. The adsorption isotherms are marked by two distinct regions of different slopes. Each region corresponds to a certain mechanism as will be described later. It was shown that the equilibrium uptake increased with increasing initial dye concentrations in the range of experimental concentrations used. Each isotherm rises sharply in the initial stages at low C_e and q_e values, thus indicating availability of plenty of readily accessible sites and a great affinity of the adsorbent for the dye molecules. The adsorbent is saturated when the plateau is reached. The decrease in the slope of the isotherm, tending to a monolayer is due to the less active sites being available at the end of the adsorption process. From Fig. 8, maximum adsorption density of QCoPz (Γ_{max}) on sepiolite and equilibrium concentration of QCoPz at the onset of plateau were calculated as 3.53 mmol g^{-1} and 4.47 mmol L^{-1} for 25 °C, 3.16 mmol g^{-1} and 4.84 mmol L^{-1} for 40 °C, 3 mmol g^{-1} and 5 mmol L^{-1} for 60 °C, respectively. This confirms that the adsorption capacity decreased with increasing temperature, thus indicating that the adsorption of QCoPz onto sepiolite was an exothermic and physical process.

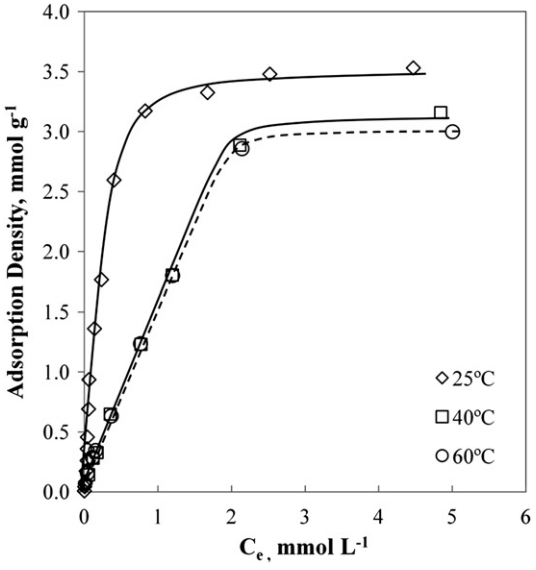

Fig. 8. Adsorption isotherm for QCoPz by sepiolite at three different temperatures (conditions: contact time = 2 h; volume = 40 ml; clay mass = 40 mg; natural pH (7–8)).

Several adsorption equilibrium theories available in the literature such as Langmuir, Freundlich, Tempkin, Redlich–Peterson and Fritz Schlunder models can be used to describe equilibrium studies. In this study, experimental data were compared by using these five well known and widely applied isotherm equations in order to find the best-fitted model for the data obtained. The different equation parameters and the underlying thermodynamic hypotheses of these models often provide insight into the adsorption mechanism, the surface properties and affinity of the adsorbent [41]. The parameters and correlation coefficients of these models for the adsorption of QCoPz on sepiolite were determined from non-linear regression (except Tempkin model) by using commercial software of Wolfram Mathematica, as summarized in Table 4.

3.6.1. The Langmuir model

The Langmuir isotherm theory assumes monolayer coverage of adsorbate over a homogenous adsorbent surface [42]. In Eq. (14), K_L (L g^{-1}) and a_L (L mmol^{-1}) are the Langmuir isotherm constants; C_e and q_e are the liquid phase concentration and solid phase concentration of adsorbate at equilibrium.

$$q_e = K_L C_e / 1 + a_L C_e \quad (11)$$

Table 4
Values of the parameters obtained from models and correlation coefficients.

Model	Constants	Temperature		
		25 °C	40 °C	60 °C
Freundlich	n	2.684E+00	1.834E+00	1.949E+00
	K_F (L mmol^{-1})	2.459E+00	1.483E+00	1.472E+00
	R^2	9.428E−01	9.647E−01	9.584E−01
	E	3.665E+00	4.261E−01	3.882E−01
	e ave	−8.459E−02	−3.809E−01	−4.467E−02
	RMSE	4.620E−01	3.045E−01	3.163E−01
Langmuir	K_L (L g^{-1})	1.473E+01	2.583E+00	2.702E+00
	a_L (L mmol^{-1})	3.784E+00	5.679E−01	6.456E−01
	q_m (mmol g^{-1})	3.898E+00	4.548E+00	4.185E+00
	R^2	9.954E−01	9.884E−01	9.851E−01
	E	7.192E−01	1.037E−01	1.245E−01
	e ave	−4.354E−02	−1.764E−01	−1.415E−02
	RMSE	1.415E−01	1.731E−01	1.862E−01
Tempkin	B_1 (J mmol^{-1})	6.170E−01	7.529E−01	6.787E−01
	K_T (L mmol^{-1})	8.602E+01	1.133E+01	1.393E+01
	R^2	9.584E−01	9.563E−01	8.403E−01
	E	8.510E+00	6.189E−01	6.407E−01
	e ave	3.789E−01	−3.805E−01	−4.100E−05
	RMSE	−5.025E−05	3.301E−01	3.488E−01
Redlich–Peterson	a_{RP} (L mmol^{-1})	2.758E+00	3.480E−02	4.254E−02
	β	1.122E+00	2.390E+00	2.310E+00
	K_{RP} (L g^{-1})	1.221E+01	1.638E+00	1.651E+00
	R^2	9.970E−01	9.995E−01	9.994E−01
	E	5.565E−01	1.140E−01	1.536E−01
	e ave	−2.601E−02	1.908E−01	3.200E−02
	RMSE	1.093E−01	4.973E−02	6.102E−02
Fritz–Schlunder	a	2.374E+01	1.544E+00	1.540E+00
	b	1.234E+00	8.466E−01	8.190E−01
	c	6.419E+00	1.330E−04	7.390E−05
	d	1.251E+00	5.563E+00	5.857E+00
	R^2	9.974E−01	9.999E−01	9.998E−01
	E	2.651E−01	2.500E−02	5.605E−02
	e ave	−8.060E−03	5.535E−03	4.613E−03
	RMSE	9.581E−02	1.275E−02	2.391E−02

The Langmuir constants, K_L and a_L are evaluated through linearization of Eq. (11):

$$C_e/q_e = 1/K_L + a_L/K_L C_e \quad (12)$$

Hence by plotting C_e/q_e against C_e it is possible to obtain the value of K_L and a_L from the intercept and slope, respectively. The theoretical monolayer capacity Q_{max} is numerically equal to (K_L/a_L). The comparison of experimental and predicted data from Langmuir model is presented in Fig. 9.

The Langmuir model can be also expressed by means of a dimensionless constant R_L, whose magnitude provides information about whether the adsorption process is spontaneous or non spontaneous. It can be calculated by using Eq. (13):

$$R_L = 1/1 + a_L C_0 \quad (13)$$

where C_0 is the initial dye concentration and a_L is the Langmuir constant. The value of R_L indicates adsorption process is irreversible when R_L is 0; favorable when R_L is between 0 and 1; linear when R_L is 1; and unfavorable when R_L is greater than 1 [43]. Values of R_L calculated at 25, 40 and 60 °C were in range between 0 and 1 which indicate that the adsorption is favorable at operation conditions studied.

3.6.2. The Freundlich model

The Freundlich expression Eq. (17) is an exponential equation and therefore, assumes that as the adsorbate concentration increases so does the concentration of adsorbate on the adsorbent surface. Theoretically, using this expression, an infinite amount of adsorption can occur [44].

$$q_e = K_F C_e^{1/n} \quad (14)$$

In this equation K_F and n are the Freundlich constants related to adsorption capacity and adsorption intensity, respectively. This expression is characterized by the heterogeneity factor, $1/n$, and so the Freundlich isotherm may be used to describe heterogeneous systems [45].

The Freundlich constants are empirical constants which depend on several environmental factors. The value of $1/n$ ranges between 0 and 1, and indicates the degree of non-linearity between solution concentration and adsorption as follows [46]: if the value of $1/n$ is equal to unity, the adsorption is linear; if the value is below unity, this implies that the adsorption process is chemical; if the value is above unity, adsorption is a favorable physical process; the more heterogeneous the surface, the closer $1/n$ value is to 0 [47]. This value is the adsorption density, and since its value is between 1 and 10, the adsorption process is considered to be satisfactory. If the n value is less than 1, then the adsorption process is chemical in nature. The opposite case indicates a physical adsorption process [48]. In our study, the values found for sepiolite was around 1.834 and 2.684, which proves that the adsorption is a spontaneous and physical process. The comparison of experimental and predicted data from Freundlich model is presented in Fig. 9.

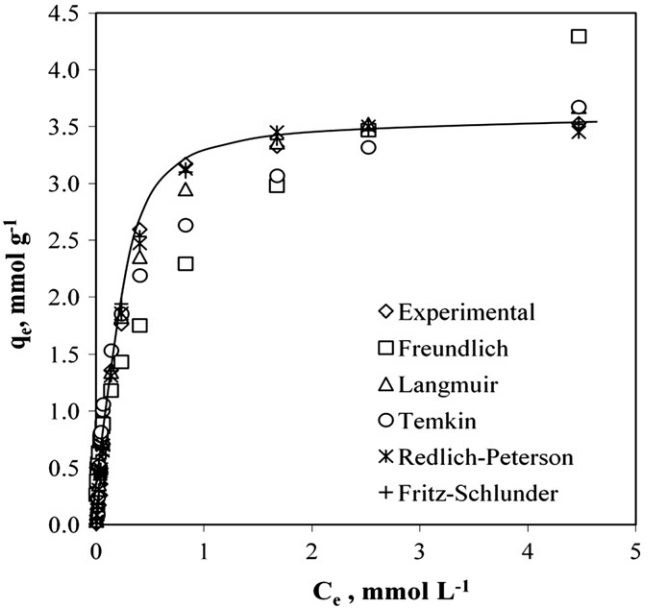

Fig. 9. Comparison of experimental and predicted adsorption isotherms of QCoPz onto sepiolite according to all analyzed models.

3.6.3. Redlich–Peterson model

Redlich and Peterson [49] have proposed an empirical equation incorporating three parameters which may be used to represent adsorption equilibria over a wide concentration range and can be applied either in homogeneous or heterogeneous systems due to its versatility. The Redlich–Peterson equation is represented by Eq. (15)

$$q_e = K_{RP} C_e / \left(1 + a_{RP} C_e^{\beta}\right) \quad (15)$$

where K_{RP} ($L\,g^{-1}$) and a_{RP} ($L\,mmol^{-1}$)are isotherm constants, and β is an exponent which lies between 0 and 1.

3.6.4. Tempkin model

Tempkin and Pyzhev [50] considered the effects of some indirect adsorbate–adsorbate interactions on adsorption isotherms and suggested that the heat of adsorption of all the molecules in the adsorbed layer would decrease linearly with coverage. Tempkin isotherm equation is given by the following equation,

$$q_e = \frac{RT}{b} \ln(K_T C_e) \quad (16)$$

Eq. (16) can be expressed in its linear form as:

$$q_e = B_1 \ln K_T + B_1 \ln C_e \quad (17)$$

where

$$B_1 = RT/b \quad (18)$$

The adsorption data can be analyzed according to Eq. (17). A plot of q_e versus ln C_e enables the determination of the isotherm constants K_T and B_1. The constant B_1 is related to the heat of adsorption ($J\,mmol^{-1}$)

3.6.5. Fritz–Schlunder model

Important four-parameter equation of Langmuir–Freundlich type was developed empirically by Fritz and Schlunder [51]. It is expressed by the equation:

$$q_e = A\,C_e^{\alpha}/1 + BC_e^{\beta} \quad \beta \text{ ve } \alpha \le 1 \quad (19)$$

where q_e is the adsorbed amount at equilibrium ($mmol\,g^{-1}$), C_e is the equilibrium concentration of the adsorbate ($mmol\,L^{-1}$), A and B are the Fritz–Schlunder parameters, and α and β are the Fritz–Schlunder equation exponents.

When the comparison curves given in Fig. 9 for sepiolite are examined experimental values are almost identical to the data obtained by Fritz–Schlunder adsorption model. Table 4 indicates that the correlation constants obtained for all temperatures and systems are close to 0.99 and that error analyses yield the lowest values. For all temperatures, the experimental data almost correlate

to the four-parameter Fritz–Schlunder isotherm equation. This good correlation is ascribed to the four-parameter nature of the model.

3.7. Thermodynamic evaluation of the adsorption process

The adsorption mechanism (i.e., chemical or physical) is often an important indicator to describe the type and level of interactions between the adsorbate and the adsorbent. If adsorption decreases with increasing temperature, it may be indicative of physical and the reverse is generally true for chemisorption. In sepiolite/QCoPz system, the decrease in adsorption with increasing temperature and fast adsorption kinetics, may suggest the presence of physical adsorption [52]. Nevertheless, this alone is not sufficient to determine the type of adsorption. The type of adsorption may be determined through thermodynamic quantities such as free energy of adsorption (ΔG_{ads}°) and the heat of adsorption (ΔH_{ads}°) both of which can be obtained from the adsorption data given in Fig. 8. A general adsorption isotherm for adsorption at the solid/liquid interface, taking into account the effect of size ratio (n) and lateral interaction coefficient (a) between adsorbed molecules, has the following form [53]:

$$\theta \cdot e^{(-2a\theta)}/(1-\theta)^n = K \cdot C \tag{20}$$

where

$$K = e^{\left(-\Delta G_{ads}^{\circ}/RT\right)}/55.5 \tag{21}$$

is the adsorbability of the adsorbate molecule at infinitively low coverage, C is the equilibrium concentration in mol L^{-1}, θ is the degree of surface coverage of the mineral with the collector molecule at (Γ/Γ_{max}); R is the gas constant (8.1314 J mol^{-1} K^{-1}), T is the temperature in K, and Γ_{max} is the adsorption density at the plateau. The free energy of adsorption can be calculated from Eq. (21) as a function of θ.

The calculation of ΔG°_{ads} has been made using five models: the Flory–Huggins [54], Frumkin [55], Modified Frumkin [56], Dubinin–Radushkevich and Langmuir equations [57]. If the adsorption data obey these equations, the above parameters, i.e., (n, a, and K) are plugged into Eqs. (20) and (21) and free energy of adsorption is calculated. The value of n in the case of the Flory–Huggins and modified Frumkin equations depend on the size of the adsorbate. The a and n value pairs for Frumkin, Modified Frumkin, Flory–Huggins, and Langmuir equations are 1,1; 2,1; 2,0; and 1,0, respectively.

For instance, by rearranging Eq. (20) and taking the logarithms for $n = 2$ and $a = 1$; the modified Frumkin equation is obtained:

$$\ln\left[\theta/C(1-\theta)^2\right] = 2a\theta + \ln K \tag{22}$$

The results of all equations are shown in Fig. 10. The slopes and intercepts of the straight lines in Fig. 10 have been used to determine the value of ΔG°_{ads} with the results presented in Table 5. While ΔG°_{ads} determines the affinity of the mineral surface towards the adsorbate

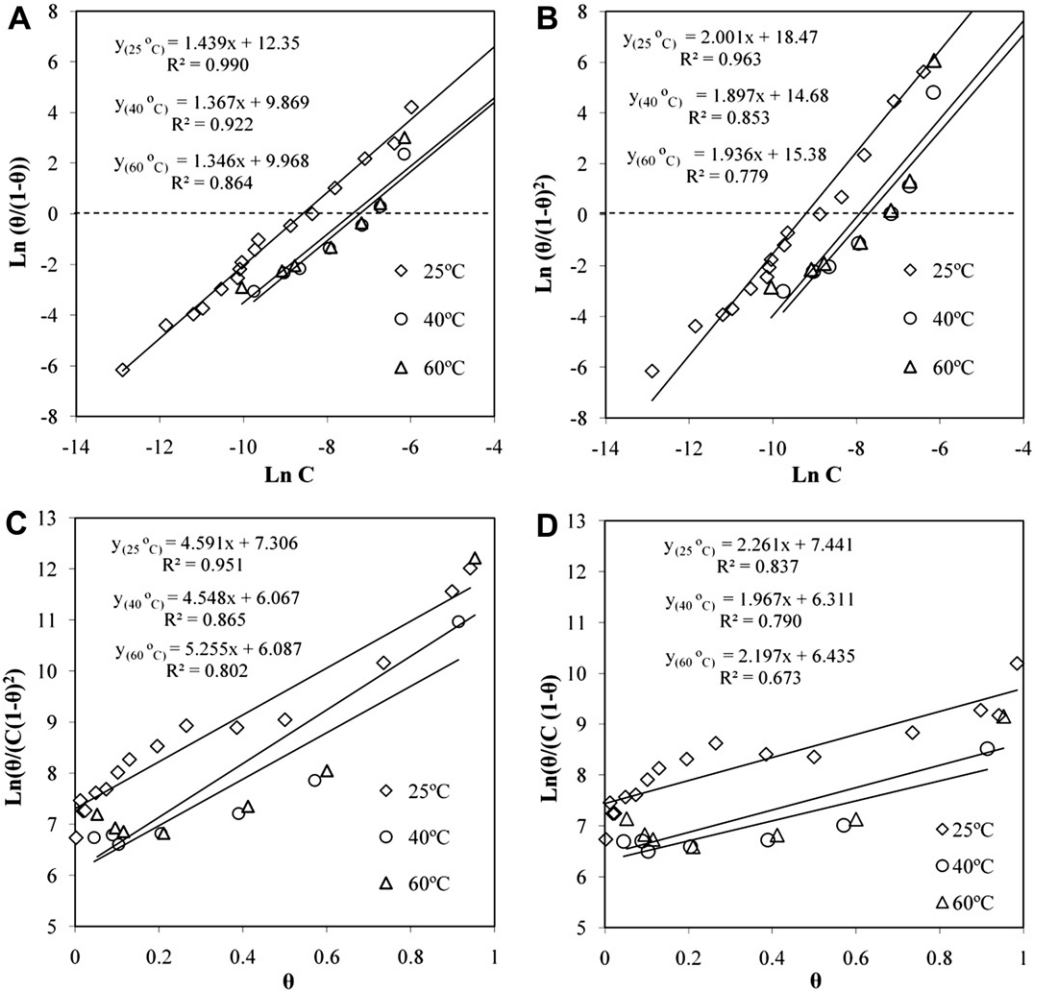

Fig. 10. Illustration of Langmuir(A), Flory–Huggins(B), modified Frumkin(C) Frumkin(D) equations based on the data in Fig. 8.

Table 5
Thermodynamic parameters for the adsorption of QCoPz on sepiolite.

Model	Constants	298 K	313 K	333 K
1000/T		3.36E+00	3.19E+00	3.00E+00
Γ_{max} (mol g^{-1})		3.50E−03	3.20E−03	3.00E−03
Langmuir	K_L (L mol^{-1})	5.35E+03	1.37E+03	1.64E+03
	Ln K_L	8.58E+00	7.22E+00	7.40E+00
	ΔG_{ads}° (kJ mol^{-1})	−3.12E+01	−2.92E+01	−3.16E+01
	ΔH_{ads}° (kJ mol^{-1})	−2.68E+01		
	$T\Delta S_{ads}^{\circ}$ (kJ K^{-1} mol^{-1})	4.46E+00	2.49E+00	4.86E+00
Flory–Huggings	K_{FH} (L mol^{-1})	1.02E+04	2.29E+03	2.83E+03
	Ln K_{FH}	9.23E+00	7.74E+00	7.95E+00
	ΔG_{ads}° (kJ mol^{-1})	−3.28E+01	−3.06E+01	−3.31E+01
	ΔH_{ads}° (kJ mol^{-1})	−2.91E+01		
	$T\Delta S_{ads}^{\circ}$ (kJ K^{-1} mol^{-1})	3.74E+00	1.50E+00	4.04E+00
Frumkin	a	1.13E+00	0.98E+00	1.10E+00
	K (L mol^{-1})	1.70E+03	5.51E+02	6.23E+02
	Ln K	7.44E+00	6.31E+00	6.44E+00
	ΔG_{ads}° (kJ mol^{-1})	−2.84E+01	−2.69E+01	−2.89E+01
	ΔH_{ads}° (kJ mol^{-1})	−2.28E+01		
	$T\Delta S_{ads}^{\circ}$ (kJ K^{-1} mol^{-1})	5.60E+00	4.09E+00	6.15E+00
Modified–Frumkin	a	2.30E+00	2.27E+00	2.63E+00
	K (L mol^{-1})	1.49E+03	4.31E+02	4.40E+02
	Ln K	7.31E+00	6.07E+00	6.09E+00
	ΔG_{ads}° (kJ mol^{-1})	−2.81+E01	−2.62E+01	−2.80E+01
	ΔH_{ads}° (kJ mol^{-1})	−2.80E+01		
	$T\Delta S_{ads}^{\circ}$ (kJ K^{-1} mol^{-1})	0.26E+00	−1.55E+00	0.17E+00
Dubinin–Radushkevich	q_m (mmol g^{-1})	0.03E+00	0.02E+00	0.01E+00
	K' (mol^2 J^{-2})	7.50E−09	7.37E−09	5.84E−09
	E (J mol^{-1})	8.17E+03	8.24E+03	9.25E+03

molecules at very low coverage, "a" represents the strength of lateral interaction forces between the QCoPz molecules adsorbed on the surface. The magnitude of "a" coefficient increases with the magnitude of coating, and indicates the intensity of the interaction. Negative values of the "a" coefficient means that there is an interaction between adsorbate molecules and generally, polar moieties of the adsorbate are interacting with each other. Positive values of "a" indicates repulsion [58,59]. As seen in Table 5, the calculated a value is low and positive for sepiolite/QCoPz. The low value indicates that the interaction in the adsorbed layer is laterally weak [60]. The positive value, on the other hand, shows that polar moieties of the adsorbate exert repulsive force to each other. The Frumkin equation and its modified form take into account both the size ratio and the lateral interaction coefficient and appears to contribute to better predictions than Langmuir and Flory–Huggins equations.

Another equation that has been used to determine the possible adsorption mechanism is the Dubinin–Radushkevick equation, which assumes a constant sorption potential [61]. The linear presentation of this equation is expressed by

$$\ln q_e = \ln Q_m - K\varepsilon^2 \quad (23)$$

$$\varepsilon = RT \ln(1 + 1/C_e) \quad (24)$$

where ε is the Polanyi potential, Q_m is the monolayer capacity (mol g^{-1}), C_e is the equilibrium concentration (mol L^{-1}), and K is the constant related to adsorption energy (mol^2 J^{-2}). The parameters Q_m and K can be obtained from the intercept and slope of the plot as shown in Fig. 11.

The mean free energy of sorption, E, is calculated by [62]

$$E = (-2K)^{-0.5} \quad (25)$$

The Dubinin–Radushkevick parameters and mean free energy are given in Table 5. The magnitude of E is useful for estimating the type

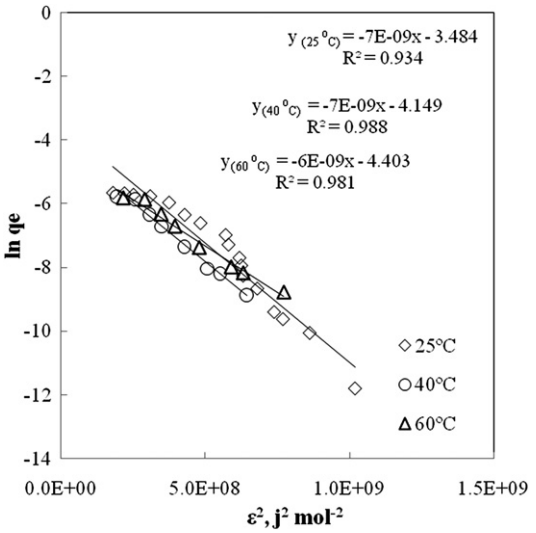

Fig. 11. Dubinin–Radushkevick plots for the adsorption of QCoPz on sepiolite.

of adsorption reaction. Generally while an energy range from 1 to 16 kJ mol^{-1} indicates adsorption process is physical, from 8 to 16 kJ mol^{-1} indicates an ion-exchange reaction [63]. Therefore, the E values obtained from the above equation (8.16–9.25 kJ mol^{-1}) are practically in the ion-exchange energy range, and thus support the idea of ion-exchange mechanism for the adsorption of QCoPz species onto sepiolite.

Another very important thermodynamic parameter in determining the type of adsorption is the heat of adsorption (ΔH_{ads}°). This can be obtained from the Clausius–Clapeyron equation [64].

$$d \ln K/d(1/T) = -\Delta H_{ads}^{\circ}/R \quad (26)$$

The slopes of ln K vs. $1/T$ are used in Eq. (26) to calculate the ΔH_{ads}° for each model, for instance a plot arranged for Flory–Huggins model is presented in Fig. 12. The overall results are presented in Table 5 along with the entropy values calculated using Eq. (27) given below:

$$\Delta G = \Delta H - T\Delta S \quad (27)$$

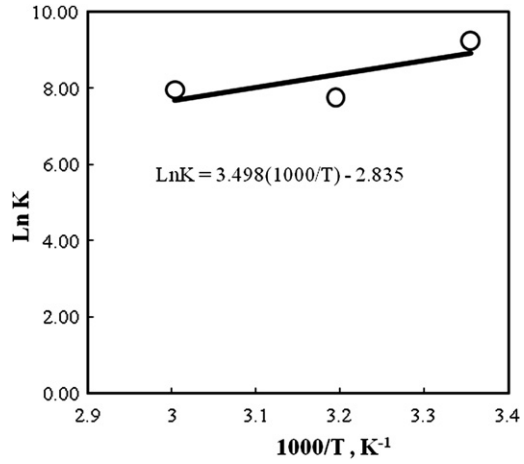

Fig. 12. Van't Hoff plot for the adsorption of QCoPz on sepiolite according to the Flory–Huggins model.

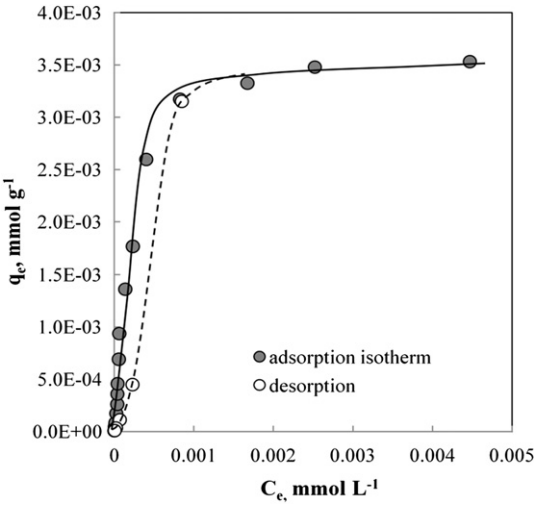

Fig. 13. Desorption plot for QCoPz/sepiolite system at 25 °C.

The negative value of free energy of adsorption calculated according to all models indicates that the adsorption of QCoPz ions onto sepiolite surface is spontaneous. The negative value of the enthalpy (Table 5) indicates that heat is released from the adsorption process. Generally, an exothermic adsorption process signifies either physi- or chemi-sorption while endothermic process is attributable unequivocally to chemisorption [65]. In an exothermic process, physisorption is distinguished form chemisorption by considering the absolute value of adsorption enthalpy. Typically, the enthalpy of a physisorption process is lower than 40 kJ mol^{-1} whereas the enthalpy of a chemisorptions process approaches 100 kJ mol^{-1} [66]. In the present case, the absolute values of enthalpy are relatively low, approaching those typical of physisorption; this conclusion is also supported by the kinetics of adsorption which was complete in less than 5 min with 99% yield. The positive value of ΔS_{ads}° indicates that there is an increase in the randomness in the system solid/solution interface during the adsorption process. Especially, in ion-exchange processes, water molecules released into the bulk solution from the solid surface cause an increase in entropy [67].

3.8. Desorption studies

Desorption studies were conducted in distilled water in order to investigate the stability of QCoPz adsorbed onto sepiolite. As mentioned in the previous section, Fig. 13 indicates that the desorption proceeds very fast in the first step, then slows down and after the fifth step the amount of QCoPz on sepiolite surface decreases by approximately 18%; this is well evident in the hysteresis curve illustrated in Fig. 13. Desorption shows that the adsorption process, occurring physically by electrostatic interaction and ion exchange, is of reversible nature. Positively charged polar terminal groups of the dye, which are adsorbed into the stern layer, interact with each other mainly repulsive in nature (based on the positive value of the constant obtained from Frumkin and modified Frumkin models). If there is a lack of negatively charged ions which will compensate for the positive charges, the repulsive forces among polar groups cause a separation of QCoPz molecules from the surface. As a result, it can be considered that QCoPz molecules on the clay surface undergo desorption in distilled water. In addition, the fast nature of this desorption process is an indication of physical adsorption of this dye onto sepiolite clay. It should be noted that ion exchange, though physical in nature, is known to be mainly irreversible.

3.9. FT-IR spectral studies of QCoPz adsorbed onto sepiolite samples

FT-IR spectroscopy is a useful tool in determining whether the adsorptive interaction between QCoPz and sepiolite is physical or chemical; FT-IR spectra of dried composites can give an idea about this interaction. Fig. 14 presents the FTIR spectrum of sepiolite. The Mg–OH band at 3718–2680 cm^{-1} characterized by low bonding strength is ascribed to the presence of OH groups in the octahedral sheet and the OH stretching vibration in the external surface of sepiolite [68]. The shoulder found at 3719 cm^{-1} is attributed to the OH stretching vibration of the silanol (Si–OH) groups [69]. On the other hand, the 3559 and 1464 cm^{-1} bands are respectively assigned to the OH stretching, representing the zeolitic water in the channels and bound water coordinated to magnesium in the octahedral sheet. The band at 1654 cm^{-1} developed due to the hydroxyl bending vibrations again reflects the presence of bound

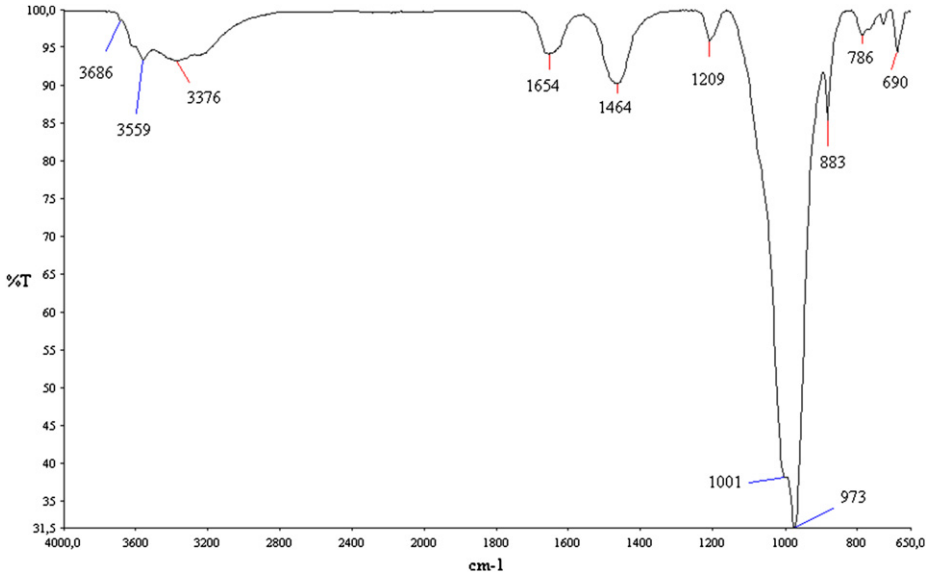

Fig. 14. IR spectrum of sepiolite sample used in this study.

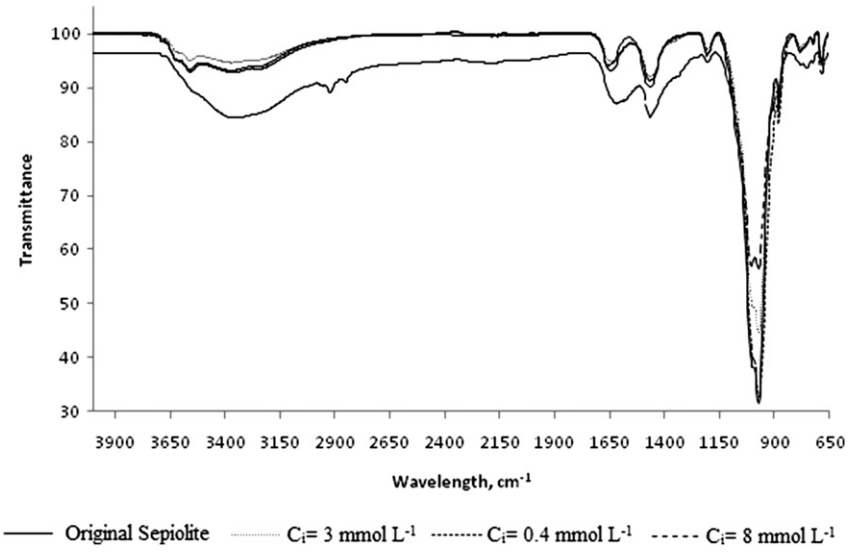

Fig. 15. Infrared spectra of sepiolite, both in pristine form and treated with varying concentrations of QCoPz solutions.

water [70]. The Si–O coordination bands at 1209, 1001, and 973 cm^{-1} form as a result of the Si–O vibrations [71].

In Fig. 15, FT-IR spectra of sepiolite adsorbed with different concentrations of QCoPz are given. These spectra show that low concentrations of the dye did not appear in the spectra, however, 8 mmol L^{-1} of starting concentration yielded signals due to the dye molecule, at 2921–2850 cm^{-1} and 1006 cm^{-1}. These signals prove the adsorption of the dye molecule.

In addition, bound and zeolitic water peaks are present in a deformed and broad fashion, which means that QCoPz molecules are either exchanged with water molecules, or coordinated with water molecules at their axial positions, or ion–dipol interactions. Bound and zeolitic water peaks, present at 1654 cm^{-1} for pure sepiolite were observed at 1621 cm^{-1} broadened, while the original peak at 1464 cm^{-1} shifted to 1470 cm^{-1} [72]. Increase in the intensity and broadening of the 3000–3600 cm^{-1} peak system probably reveals that water molecules are coordinated at the axial positions of the cobalt metal center during the adsorption process.

IR spectra given in Fig. 15 clearly indicate that none of the dye containing clay samples showed any peaks related to a chemical (covalent) bond. This is also an indication of the physical adsorption behavior of the dye molecule.

3.10. Mechanism of the adsorption process

The adsorption isotherms in Fig. 8 show mainly two distinct regions, each characterized by different adsorption rates and mechanisms. In the first stage, adsorption takes place at a lower rate and is governed by an ion-exchange process and electrostatic interactions. However, the adsorption continues to take place with increasing QCoPz concentration. In the second stage, the adsorption is mainly characterized by strong π–π aggregates and electrostatic interactions, but the ion-exchange process still continues to take place at a lower rate as the magnesium release (Fig. 16) continues even in the plateau region. The ion-exchange mechanism of QCoPz onto sepiolite can be depicted in Scheme 1 [25].

The free energy of adsorption (ΔG_{ads}°) is composed of a number of contributing forces. Among them, ΔG_{elec}°, ΔG_{solv}°, $\Delta G_{ion\text{-}exchange}^{\circ}$ and ΔG_{agg}° are relevant [73,74]. Here ΔG_{elec}° is the electrostatic contribution to the total energy which occurs between quaternary ammonium groups of the QCoPz and negatively charged sepiolite surfaces, ΔG_{agg}° represents the interaction due to association of porphyrazine molecules (aggregation) at the interface, ΔG_{solv}° is the contribution of the solvation effects on the polar head of the adsorbate, and $\Delta G_{ion\text{-}exchange}^{\circ}$ represents the exchange of similar ions (e.g., cations or anions) on the surface with QCoPz.

In our system, $\Delta G_{ion\text{-}exchange}^{\circ}$, ΔG_{elec}° and ΔG_{agg}° are responsible for the adsorption reactions in the first and second regions of the adsorption isotherm. Ion exchange occurs among Mg^{2+} ions on the surface, within the octahedral sheet and positively charged QCoPz ammonium groups in the bulk. The formation of hydrogen bond between the zeolitic water and bound water has been proposed for a number of cationic adsorbate systems such as primary amines [75]. However, the quaternary ammonium groups, which are surrounded by electron-donating CH_3 constituents and the absence of vacant electrons, make it impossible for the hydrogen bond formation.

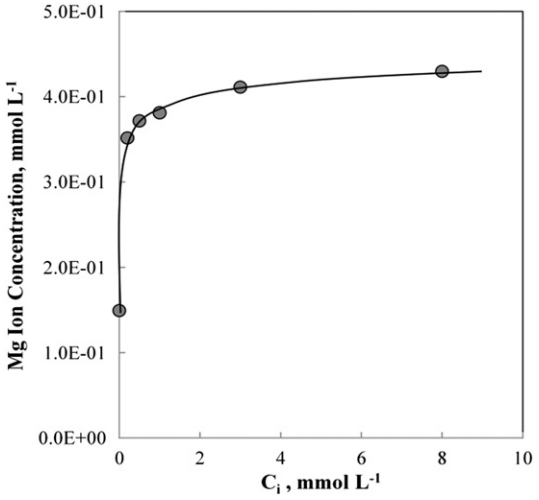

Fig. 16. The released magnesium ion concentration as a function of initial QCoPz concentration under the adsorption conditions of Fig. 8.

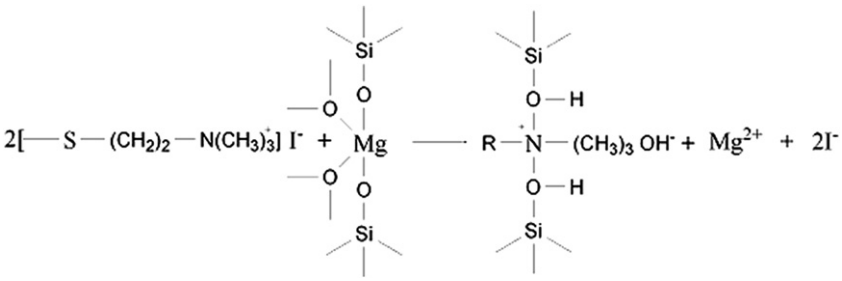

Scheme 1. Ion exchange mechanism of QCoPz onto sepiolite

The significant increase in magnesium ion concentration in Fig. 16 and ion exchange isotherm in Fig. 17 clearly shows that ion-exchange mechanism is the one responsible for the adsorption until nearly 2.67×10^{-2} mmol L^{-1} equilibrium concentration. At this point, calculations made by using Eq. (30) yielded that 73% of the adsorption proceeded through ion exchange whereas electrostatic interaction remained at 27% [76]. However, adsorption through electrostatic interactions increased with increasing equilibrium concentration; for example, at 4.36×10^{-2} mmol L^{-1} equilibrium dye concentration, 71% and at 6.47×10^{-2} mmol L^{-1}, 85% of total adsorption is due to electrostatic means. Here, it is normal to expect low ion exchange because sepiolite is characterized by low cation exchange capacity. These results indicate that ion exchange mechanism proceeds very fast in the beginning of the adsorption process, and then electrostatic interactions takes over approaching the plateau region (Fig. 17). The significant increase in the slope of adsorption isotherm in the second region is ascribed to the aggregation through π–π interactions among the adsorbed QCoPz molecules.

$$\%\text{Ion Exchange} = \frac{Z_{Mg} \times \text{Amount of Magnesium in solution}}{Z_{QCoPz} \times \text{Amount of adsorbed QCoPz}} \times 100 \quad (Z = \text{Valence of ions}) \tag{28}$$

The calculations made using Eq. (28) and results given in Fig. 17 show good agreement with the desorption behavior of QCoPz. In addition, the average pore size of sepiolite used in this study is about 37 Å and the diameter of the ammonium polar head is 5.69 Å. This indicates that polar heads of QCoPz encounter no difficulty to be accommodated in the pores of sepiolite. It should be noted that the whole molecule needs not to get into the pore but rather the polar part [25].

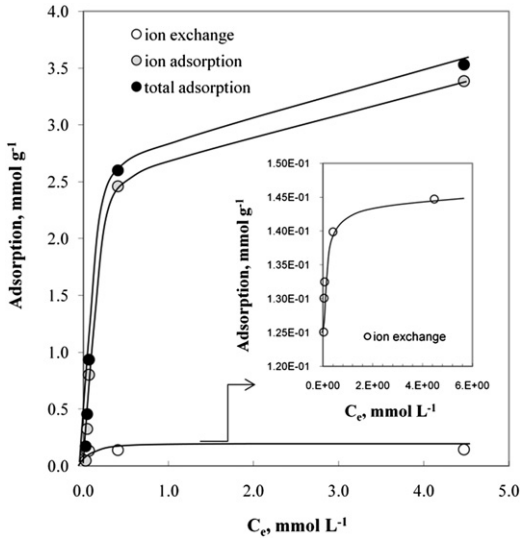

Fig. 17. Ion exchange, electrostatic and total adsorption isotherms of QCoPz/sepiolite system.

4. Conclusion

The adsorption of cationic tetrapyrrole derivative QCoPz onto sepiolite has been investigated. The following remarkable points are obtained.

An optimum solid concentration of 0.1% with a mixing time of two hours was found to be sufficient for reaching equilibrium in sepiolite/QCoPz system. Zeta potential measurements yielded that adsorption of cationic QCoPz compound onto sepiolite shifted the zeta potential of the sepiolite from negative to positive value; this indicates that the cationic dye adsorbed onto negatively charged clay surface through either electrostatic or other mechanisms. Adsorption kinetics studies revealed that pseudo second-order model fits best the sepiolite/QCoPz system with the highest constant and lowest error analyses values.

Adsorption of cationic QCoPz on sepiolite exhibits two distinct regions. The first stage is characterized by low rate and governed through ion exchange process between ammonium ions and magnesium ions in the octahedral sheet together with electrostatic interactions between negatively charged surface and cationic groups in the adsorbate molecule. The second stage is ascribed to a combination of π–π interactions due to aggregation of porphyrazine rings and electrostatic interactions. In sepiolite/QCoPz system, the decrease in adsorption with increasing temperature and fast adsorption kinetics, may suggest the presence of physical adsorption. Maximum adsorption capacity of sepiolite for QCoPz adsorption is found to be 3.53 mmol g^{-1} at 25 °C, 3.16 mmol g^{-1} at 40 °C, 3 mmol g^{-1} at 60 °C, respectively.

Five isothermal models, applied to the experimental data, yielded that the most suitable model at different temperatures was the Fritz–Schlunder model in terms of all calculated parameters and error analysis data. The data obtained from adsorption isotherms at different temperatures were fit to various adsorption models to calculate thermodynamic quantities such as the free energy of adsorption, heat of adsorption and entropy of adsorption. The results indicate that QCoPz adsorption onto sepiolite is spontaneous and physical in nature. Also from Dubinin–Radushkevich model, the *E* values obtained from (8.16–9.25) kJ mol^{-1} that are practically in the range of physical adsorption supporting the adsorption of QCoPz species onto sepiolite as mainly physical in nature. Desorption studies resulted in 18% decrease of QCoPz from sepiolite surface.

The novel QCoPz/sepiolite composite is likely to be used in green chemistry and a wide range of optical and catalytic applications especially those crucially important to the petroleum industry, waste water cleaning, pulp/paper industry and removal of odour.

Acknowledgement

This work was supported by the Research Fund of the Technical University of Istanbul.

References

[1] Kadish KM, Smith KM, Guilard R. In: The porphyrin handbook, vol. 17. , San Diego: Academic Press; 2003. p. 247–85.
[2] Kadish KM, Smith KM, Guilard R, editors. The porphyrin handbook, vol. 6. San Diego: Academic Press; 2000. p. 43–132.
[3] Arslanoğlu Y, Sevim AM, Hamuryudan E, Gül A. Near-IR absorbing phthalocyanines. Dyes and Pigments 2006;68(2-3):129–32.
[4] Nyman ES, Hynninen PH. Research advances in the use of tetrapyrrolic photosensitizers for photodynamic therapy. Journal of Photochemistry and Photobiology 2004;B73(1-2):1–28.
[5] Drain CM, Hupp JT, Suslick KS, Wasielewski MR, Chen X. A perspective on four new porphyrin-based functional materials and devices. Journal of Porphyrins and Phthalocyanines 2002;6(4):243–8.
[6] Wöhrle D, Suvorova O, Gerdes R, Bartels O, Lapok L, Baziakina N, et al. Efficient oxidations and photooxidations with molecular oxygen using metal phthalocyanines as catalysts and photocatalysts. Journal of Porphyrins and Phthalocyanines 2004;8:1020–41.
[7] Barloy L, Battioni P, Mansuy D. Manganese porphyrins supported on montmorillonite as hydrocarbon monooxygenation catalysts: particular efficacy for linear alkane hydroxylation. Journal of the Chemical Society, Chemical Communications; 1990:1365–7.
[8] Barloy L, Lallier JP, Battioni P, Mansuy D, Piffard Y, Tournoux M, et al. Manganese porphyrins adsorbed or intercalated in different mineral matrixes: preparation and compared properties as catalysts for alkene and alkane oxidation. New Journal of Chemistry 1992;16(1–2):71–80.
[9] Ortiz de Montenallo PR. Cytochrome P-450: structure, mechanism and biochemistry. New York: Plenum Press; 1986.
[10] Meunier B. Metalloporphyrins as versatile catalysts for oxidation reactions and oxidative DNA cleavage. Chemical Reviews 1992;92(6):1411–56.
[11] Bedioui F, Gaillon L, Devynck J, Battioni P. Electroassisted biomimetic oxidation of hydrocarbons by molecular oxygen catalyzed by manganese porphyrin complexes intercalated into montmorillonite. Journal of Molecular Catalysis 1993;78(2):L23–6.
[12] Bedioui F. Zeolite-encapsulated and clay-intercalated metal porphyrin, phthalocyanine and Schiff-base complexes as models for biomimetic oxidation catalysts: an overview. Coordination Chemistry Reviews 1995;144: 39–68.
[13] Sakoda K, Kominami K. Photochemical hole burning of cationic porphin/saponite intercalation compounds. Chemical Physics Letters 1993;216(3-6):270–4.
[14] Sasai R, Sugiyama D, Takahashi S, Tong Z, Shichi T, Itoh H, et al. The removal and photodecomposition of n-nonylphenol using hydrophobic clay incorporated with copper phthalocyanine in aqueous media. Journal of Photochemistry and Photobiology A: Chemistry 2003;155(1-3):223–9.
[15] Takagi S, Shimada T, Yui T, Inoue H. High density adsorption of porphyrins onto clay layer without aggregation: characterization of smectite-cationic porphyrin complex. Chemistry Letters 2001;2:128–9.
[16] Takagi S, Tryk DA, Inoue H. Photochemical energy transfer of cationic porphyrin complexes on clay surface. The Journal of Physical Chemistry B 2002;106(21):5455–60.
[17] Brauner K, Preisinger A. Struktur und Entstehung des Sepioliths. Tschermaks Mineralogische und Petrographische Mitteilungen 1956;6:120–40.
[18] Brindley GW. X-ray and electron diffraction data for sepiolite. American Mineralogist 1959;44:495–500.
[19] Alvarez A. Sepiolite: properties and uses. In: Singer A, Galan E, editors. Developments in sedimentology. , Amsterdam: Elsevier; 1984. p. 253–85.
[20] Lomauro CJ, Bakshi AS, Labuza TP. Evaluation of food moisture sorption isotherm equations. Part II: milk, coffee, tea, nuts, oilseeds, spices and starchy foods. Lebensmittel-Wissenschaft und -Technologie 1985;18:118–24.
[21] Can MF. Ph.D. dissertation. Production of sepiolite/epoxy nanocomposite and its characterization, Istanbul Tech. Univ, Turkey.
[22] Çınar M, Sabah E, Çelik MS. Rheological properties of sepiolite ground in acid and alkaline media. Applied Clay Science 2009;42(3–4):422–6.
[23] Al-Degs Y, Khraisheh MAM, Allen SJ, Ahmad MN. Effect of carbon surface chemistry on the removal of reactive dyes from textile effluent. Water Research 2000;34(3):927–35.
[24] Sabah E, Çelik MS. Adsorption mechanism of quaternary amines by sepiolite. Separation Science and Technology 2002;37(13):3081–97.
[25] Polat M, Gül A. Synthesis of new porphyrazines with tertiary or quaternized aminoethyl substituents. Dyes and Pigments 2000;45(3):195–9.
[26] Kavran G, Akkuş H, Gül A, Erim FB. Separation of positional isomers of aromatic anions by capillary electrophoresis using quarternized porphyrazine ion in aqueous solution. Journal of Separation Science 2002;25:1–6.
[27] Alvarez A. In: Singer A, Galan E, editors. Palygorskite-sepiolite occurences, genessis and uses, sepiolite: properties and uses; developments in sedimentology., vol. 37. Amsterdam: Elsevier; 1984. p. 253–87.
[28] Matis KA. Flotation science and technology. New York: Marcel Dekker Inc.; 1995.
[29] Wakamatsu T, Fuerstenau DW. Effect of alkyl sulfonates on the wettability of alumina. The AIME Transactions 1973;254:123.
[30] Demirbaş O, Alkan M, Doğan M, Turhan Y, Namli H, Turan P. Electrokinetic and adsorption properties of sepiolite modified by 3-aminopropyltriethoxysilane. Journal of Hazardous Materials 2007;149(3):650–6.
[31] Erdinç A. Sorption and destruction of veterinary antibiotics on natural minerals. MSc dissertation, Boğaziçi Univ, Turkey; 2009.
[32] Aksu Z, Karabayır G. Comparison of biosorption properties of different kinds of fungi for the removal of Gryfalan Black RL metal-complex dye. Bioresource Technology 2008;99(16):7730–41.
[33] Lagergren S. Zur theorie der sogenannten adsorption geloster stoffe. Kungliga Svenska Vetenskapsakademiens. Handlingar 1898;24:1–39.
[34] Vadivelan V, Kumar KV. Equilibrium, kinetics, mechanism, and process design for the sorption of methylene blue onto rice husk. Journal of Colloid and Interface Science 2005;286(1):90–100.
[35] Gerente C, Lee VKC, Le Cloirec P, Mckay G. Application of chitosan for the removal of metals from wastewaters by adsorption-mechanisms and models-review. Critical Reviews in Environmental Science and Technology 2007;37:41.
[36] Doğan M, Alkan M, Türkyılmaz A, Özdemir Y. Kinetics and mechanism of removal of methylene blue by adsorption onto perlite. Journal of Hazardous Materials 2004;B109(1–3):141–8.
[37] Khraisheh MAM, Al-Degs YS, Allen SJ, Ahmad MN. Elucidation of controlling steps of reactive dye adsorption on activated carbon. Industrial and Engineering Chemistry Research 2002;41:1651–7.
[38] Poots V, McKay G, Healy JJ. The removal of acid dye from effluent using natural adsorbents. I. Peat. Water Research 1976;10(12):1061–6.
[39] Amin NK. Removal of direct blue-106 dye from aqueous solution using new activated carbons developed from pomegranate peel: adsorption equilibrium and kinetics. Journal of Hazardous Materials 2009;165(1–3):52–62.
[40] Gimbert F, Morin-Crini N, Renault F, Badot PM, Crini G. Adsorption isotherm models for dye removal by cationized starch-based material in a single component system: error analysis. Journal of Hazardous Materials 2008;157 (1):34–46.
[41] Özdemir AB, Turan M, Çelik MS. Adsorption of negatively charged azo dyes onto surfactant-modified sepiolite. Journal of Environmental Engineering 2003;129(8):709–15.
[42] Langmuir I. Adsorption of gases on plane surfaces of glass, mica and platinum. Journal of the American Chemical Society 1918;40:1361–403.
[43] Leechart P, Nakbanpote W, Thiravetyan P. Application of 'waste' wood-shaving bottom ash for adsorption of azo reactive dye. Journal of Environmental Management 2009;90:912–20.
[44] Freundlich H. Űber die Adsorption in Lösungen. Zeitschrift für Physikalische Chemie 1906;57:385–470.
[45] Al-Duri B, McKay G. Basic dye adsorption on carbon using a solid phase diffusion model. Chemical Engineering Journal 1988;38:23–31.
[46] Treybal RE. Mass transfer operations. New York: McGrawHill; 1987.
[47] Al-Duri B. In: McKay G, editor. Use of adsorbents for the removal of pollutants from wastewaters. CRC Press; 1996. p. 133–73 (Chapter 7).
[48] Wu CH. Adsorption of reactive dye onto carbon nanotubes: equilibrium, kinetics and thermodynamics. Journal of Hazardous Materials 2007;144 (1–2):93–100.
[49] Redlich O, Peterson DL. A useful adsorption isotherm. The Journal of Physical Chemistry 1959;63:1024–6.
[50] Tempkin MJ, Pyzhev V. Kinetics of ammonia synthesis on promoted iron catalysts. Acta Physiochimica USSR 1940;12:217–22.
[51] Fritz W, Schlunder EU. Simultaneous adsorption equilibria of organic solutes in dilute aqueous solution on activated carbon. Chemical Engineering Science 1974;29:1279–82.
[52] Sabah E, Sağlam H, Kara M, Çelik MS. Uptake of cationic surfactants by a clay absorbent: sepiolite. In: Proceedings of southern hemisphere meeting, Buenos Aires, May 6–9, 1997, p. 277–80.
[53] Yehia A, Miller JD, Ateya BG. Analysis of the adsorption behavior of oleate on some synthetic apatites. Minerals Engineering 1993;6:79–86.
[54] Dhar HP, Conway BE, Joshi KM. Form of adsorption isotherms for substitutional adsorption of molecules of different sizes. Electrochimica Acta 1973;18 (11):789.
[55] Grchev T, Cvetkovska M, Stafilov T, Schultze JW. Adsorption of polyacrylamide on gold and iron from acidic aqueous solutions. Electrochimica Acta 1991;36:1315.
[56] Frumkin AN, Damaskin BB. In: Bockris JO'M, Conway BE, editors. Modern aspects of electrochemistry, vol. 3. London: Butterworths; 1964. p. 149–223.
[57] Quan C, Khoe G, Bagster D. Adsorption of lauryl sulfate onto arsenic-bearing ferrihydrite. Water Research 2001;35(2):478–84.
[58] Sabah E. Adsorption mechanism of quaternary amines by sepiolite. Ph.D. dissertation, Osmangazi Univ: Turkey; 1998.
[59] Kara M, Yüzer H, Sabah E, Çelik MS. Adsorption of cobalt from aqueous solutions onto sepiolite. Water Research 2003;37(1):224–32.
[60] Martinez S, Stern I. Thermodynamic characterization of metal dissolution and inhibitor adsorption processes in the low carbon steel/mimosa tannin/sulfuric acid system. Applied Surface Science 2002;199(1–4):83–9.

[61] Krishna BS, Murty DSR, Prakash BSJ. Thermodynamics of chromium(VI) anionic species sorption onto surfactant-modified montmorillonite clay. Journal of Colloid Interface Science 2000;229(1):230–6.
[62] Juang RS, Lin SH, Tsao KH. Mechanism of sorption of phenols from aqueous solutions onto surfactant-modified montmorillonite. Journal of Colloid Interface Science 2002;254(2):234–41.
[63] Helfferich F. Ion exchange. New York: McGraw Hill; 1962.
[64] Çelik MS, Yoon RH. Adsorption of poly(Oxyetyhylene)nonylphenol homologues on a low-ash coal. Langmuir 1991;7:79–86.
[65] Durnie W, De Marco R, Kinsella B, Jefferson A. Development of a structure-activity relationship for oil field corrosion inhibitors. Journal of the Electrochemical Society 1999;146(5):1751.
[66] Brdička R. Osnove Fizikalne Kemije. Zagreb: Školska knjiga; 1965. 460–461.
[67] Xin H, Nai-yun G, Qiao-li Z. Thermodynamics and kinetics of cadmium adsorption onto oxidized granular activated carbon. Journal of Environmental Sciences 2007;19(11):1287–92.
[68] Rytwo G, Nir S, Margulies B, Casal B, Merino J, Ruiz-Hitzky E, et al. Adsorption of monovalent organic cations on sepiolite: experimental results and model calculations. Clays and Clay Minerals 1998;46(3):340.
[69] Akyüz S, Akyüz T, Yakar AE. FT-IR spectroscopic investigation of adsorption of 3-aminopyridine on sepiolite and montmorillonite from Anatolia. Journal of Molecular Structure 2001;565–566:487–91.
[70] Ahlrichs JL, Serna C, Serratosa JM. Structural hydroxyls in sepiolites. Clays and Clay Minerals 1975;23(2):119–24.
[71] Cornejo J, Hermosin MC. Structural alteration of sepiolite by dry grinding. Clay Minerals 1988;23:391–8.
[72] Sabah E, Çelik MS. Interaction of pyridine derivatives with sepiolite. Journal of Colloid and Interface Science 2002;251(1):33–8.
[73] Fuerstenau DW, Raghavan S. In: Fuerstenau MC, editor. Flotation. A.M. Gaudin memorial volume; some aspects of the thermodynamics of flotation, vol. 1. New York: AIME Publication; 1976. p. 21–65.
[74] Çelik MS, Somasundaran P. Effect of chain length on dissolution of calcium sulfonate precipitates. Journal of Colloid and Interface Science 1988;122:163–70.
[75] Shuali U, Bram L, Steinberg M, Yariv S. Infrared study of the thermal treatment of sepiolite and palygorskite saturated with organic acids. Thermochimica Acta 1989;148:445–56.
[76] Gülgönül İ. Mechanisms of mono and multi valent ions on the separation of sodium and potasium feldspars in cationic flotation method. Ph.D. dissertation, Istanbul Tech. Univ., Turkey; 2004.